

Anisotropic magnetic properties of trigonal ErAl_2Ge_2 single crystal

Moumita Nandi[✉], A Thamizhavel[✉] and S K Dhar[✉]

Department of Condensed Matter Physics and Materials Science, Tata Institute of Fundamental Research,
Dr. Homi Bhabha Road, Colaba, Mumbai, 400 005, India

E-mail: moumita.nandi11@gmail.com

Received 18 November 2019, revised 24 December 2019

Accepted for publication 17 January 2020

Published 6 February 2020



Abstract

We report the anisotropic magnetic properties of the ternary compound ErAl_2Ge_2 . Single crystals of this compound were grown by high temperature solution growth technique, using Al:Ge eutectic composition as flux. From the powder x-ray diffraction we confirmed that ErAl_2Ge_2 crystallizes in the trigonal CaAl_2Si_2 -type crystal structure. The anisotropic magnetic properties of a single crystal were investigated by measuring the magnetic susceptibility, magnetization, heat capacity and electrical resistivity. A bulk antiferromagnetic ordering occurs around 4 K as inferred from the magnetic susceptibility and the heat capacity. The susceptibility is larger along the ab -plane and flattens out below the magnetic transition temperature (T_N) and the magnetization in the ordered state increases more rapidly along the ab -plane than along the c -axis suggesting that the moments are inclined more towards the ab -plane. The magnetic susceptibility, magnetization and the $4f$ -derived part of the heat capacity in the paramagnetic regime analysed based on the point charge model of the crystalline electric field (CEF) indicate a relatively low CEF energy level splitting.

Keywords: ErAl_2Ge_2 , magnetocrystalline anisotropy, single crystal, antiferromagnetism

(Some figures may appear in colour only in the online journal)

1. Introduction

The rare-earth intermetallic compounds of the general formula RT_2X_2 , where R is the rare-earth, T is a transition metal and X is a p -block element, crystallizing in the ThCr_2Si_2 -type crystal structure have been investigated extensively owing to their interesting physical properties like superconductivity, heavy fermion behaviour, valence fluctuation, magnetic ordering etc [1–5]. A lesser number of rare-earth based compounds with the general formula (1-2-2) crystallize in the trigonal CaAl_2Si_2 -type crystal structure. The reason for their relative paucity is that the number of valence electrons should not exceed 16 [6, 7], which is satisfied by a lesser number of compositions. However, it has been found that RAl_2X_2 ($X = \text{Si}$ and Ge) compounds, where valence electron count is 17, are exceptions to this rule [7, 8]. Kranenberg *et al* attributed the stability of these compounds to the small electronegativity differences between the Al and Si (Ge) atoms.

The RAl_2X_2 compounds crystallizing in the CaAl_2Si_2 -type structure adopt the $P\bar{3}m1$ space group (#164). An interesting feature of this structure type is that the rare-earth atoms form a triangular lattice in the ab -plane and the layers formed by Al and Si atoms are separated by distance c , the lattice parameter normal to the hexagonal plane. The RAl_2X_2 ($R = \text{Eu}$ and Yb ; $X = \text{Si}$ and Ge) have been previously investigated in the polycrystalline form [7, 9]. We have reported the physical properties of EuAl_2Si_2 single crystal [10], which orders antiferromagnetically at 33 K and exhibits a substantially large magnetoresistance (1200% at 14 T) at 2 K for the field applied along the c -axis. Very recently, we reported the magnetic properties of HoAl_2Ge_2 single crystal [11] which undergoes a bulk antiferromagnetic transition at 6.5 K with the ab -plane as the easy plane of magnetization. In continuation of our studies on this series of compounds we have successfully grown the single crystals of ErAl_2Ge_2 and probed the magnetic behavior using the techniques of magnetization, electrical resistivity and heat capacity.

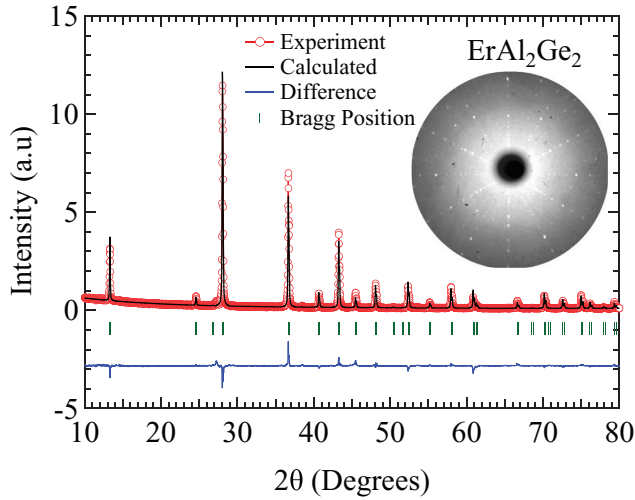


Figure 1. Rietveld refinement of the powder x-ray diffraction pattern of crushed single crystals of ErAl_2Ge_2 . Inset shows the Laue diffraction pattern corresponding to the (001) plane.

2. Experimental methods

Single crystals of ErAl_2Ge_2 were grown by the high temperature solution growth method, taking advantage of the deep eutectic (420 °C) formed by the Al:Ge (72:28) [12]. High purity metals of Er, Al and Ge with a starting composition of 1 : 17.5 : 7.5 were placed in a high quality recrystallized alumina crucible. The alumina crucible was sealed in an evacuated quartz ampoule under a partial pressure of argon gas. The pressure of the argon gas was kept at a level such that it does not exceed the atmospheric pressure at the maximum growth temperature. The ampoule was placed in a resistive heating box type furnace and heated to 1050 °C at a rate of 30 °C h⁻¹ and held at this temperature for 20 hr for homogenizing the melt. Then the furnace was cooled at the rate of 1.8 °C h⁻¹ down to 600 °C at which point the excess flux was removed by means of centrifuging. Well defined shiny single crystals with typical dimensions of 4 mm × 3 mm × 1 mm were obtained. A few pieces of the single crystals were ground for powder x-ray diffraction measurement using PANalytical x-ray machine with a monochromatic Cu-K α radiation. The crystals were oriented along *ab*-plane and along *c*-axis by means of Laue diffraction, in the back-reflection geometry, using a polychromatic source of x-rays. The magnetic measurements were performed using SQUID magnetometer (Quantum Design, USA) and the heat capacity and electrical measurements were performed using a physical property measurement system (PPMS).

3. Results and discussions

3.1. X-ray studies

The room temperature powder x-ray diffraction (XRD) pattern of ErAl_2Ge_2 is shown in figure 1. All the peaks can be indexed to the trigonal CaAl_2Si_2 type crystal structure and there are no extra peaks due to any trace impurity phase(s). The Rietveld analysis of the XRD data furnishes the lattice constants as $a = 4.180$ Å and $c = 6.654$ Å, which are in close

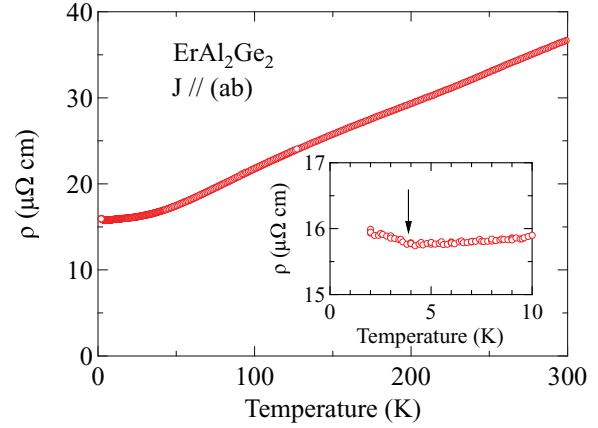


Figure 2. Temperature dependence of electrical resistivity with current in the basal plane. The inset shows low temperature region where the magnetic ordering is indicated by an arrow.

agreement with the previously reported values [13]. The well defined Laue diffraction pattern, shown in the inset of figure 1 confirms the good quality of the single crystal. The nearest Er–Er distance is in the *ab*-plane which is the same as that of the lattice constant *a*.

3.2. Electrical resistivity

The temperature dependence of electrical resistivity was measured from 2–300 K by passing a current of 1 mA in the *ab*-plane of the crystal and is shown in figure 2. The electrical resistivity decreases with the decrease in temperature typical of a metal and shows an upturn below 4 K, which is due to the onset of antiferromagnetic ordering (see magnetization data below). Similar upturn in the electrical resistivity was observed in the isostructural compound HoAl_2Ge_2 [11], below its Néel temperature. The increase in the electrical resistivity in the antiferromagnetic state is usually attributed to the formation of superzone gap, when the magnetic periodicity is different from the lattice periodicity. Because of the gap opening the number of charge carrier decreases which leads to the increase in the electrical resistivity. The superzone gap is observed in elemental rare-earth metals such as Dy, Er, Ho and Tm etc [14] and has also been observed in several rare-earth intermetallic compounds like CeGe, CePd₅Al₂, UCu₂Sn, UNiGa etc to name a few [15–18].

3.3. Magnetic susceptibility and isothermal magnetization

3.3.1. Magnetic susceptibility. The *dc* magnetic susceptibility (main panel) measured in an applied field of 3 kOe and the inverse magnetic susceptibility (inset) of ErAl_2Ge_2 are shown in figure 3. The susceptibility follows Curie–Weiss behaviour at high temperatures. There is a prominent change of slope in the susceptibility at around 4 K for field applied both along the *c*-axis and normal to it, which is due to the antiferromagnetic transition at 4 K. A large anisotropy is observed at low temperatures (below 20 K) but it weakens considerably at higher temperature in the paramagnetic state. The susceptibility in the *ab*-plane increases more rapidly below 20 K than

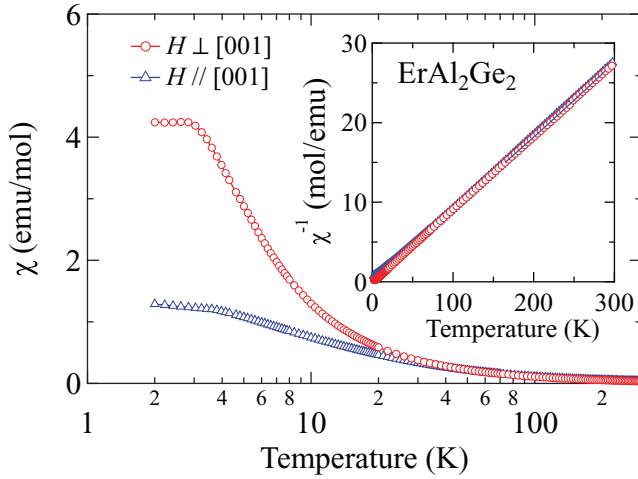


Figure 3. Temperature dependence of the magnetic susceptibility for field parallel and perpendicular to the ab -plane. The inset shows the inverse susceptibility plot along with the modified Curie–Weiss fit.

along the c -axis, thus indicating that the easy axis of magnetization is inclined more towards the ab -plane. Similar behaviour was previously observed in HoAl_2Ge_2 [11]. The inverse susceptibility data were fitted to the modified Curie–Weiss law, $\chi^{-1} = (\chi_0 + \frac{C}{T - \theta_p})^{-1}$, where χ_0 is the temperature independent term whose contributions come from the core-electrons and the Pauli spin susceptibility of the conduction electrons. We obtain an effective magnetic moment of $9.73 \mu_B/\text{Er}$ and $9.31 \mu_B/\text{Er}$ and the paramagnetic Curie–Weiss temperature of -7.35 K and -0.39 K for $H \parallel ab$ -plane and c -axis, respectively. The effective magnetic moment values are close to the Hund’s rule derived value of $9.59 \mu_B/\text{Er}$ for free Er^{3+} . If we compare the overall magnetic susceptibility with that of HoAl_2Ge_2 , the anisotropy in paramagnetic state is relatively weaker for ErAl_2Ge_2 . This can be attributed to the crystal electric field (CEF) effect. A similar behavior is observed in R_2CoGa_8 ($\text{R} = \text{Gd-Lu}$), where the sign of the B_2^0 parameter (discussed later) changes as one moves towards higher rare-earth side [19].

3.3.2. Magnetization. The isothermal magnetization measured at $T = 2 \text{ K}$ is shown in figure 4 for field parallel to ab -plane and c -axis, respectively. The magnetization increases more rapidly in the ab -plane at low fields and shows signs of gradual saturation as the field is increased above 10 kOe. On the other hand, for $H \parallel c$ -axis the magnetization in comparison initially increases less rapidly at low fields and it is less than the corresponding value for $H \parallel ab$ up to a field of 85 kOe beyond which the magnetization along the c -axis crosses that of ab -plane thus indicating the change in easy axis at high magnetic fields. It is interesting to mention here that the calculated magnetization based on a crystalline electric field model (to be discussed later) also exhibits a cross-over at slightly higher fields thus qualitatively matching with the experimental data as shown in figure 4(b). The overall field dependence of magnetization behavior suggests an antiferromagnetic ordering in ErAl_2Ge_2 . At 140 kOe, the

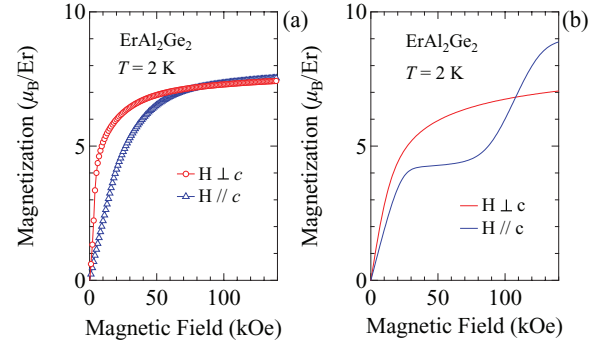


Figure 4. (a) Isothermal magnetization at $T = 2 \text{ K}$ for $H \parallel (ab)$ -plane and $H \parallel c$ -axis for fields up to 14 T. (b) Simulated magnetization plots with the CEF parameters (see text for details).

magnetization attains a value of $7.43 \mu_B/\text{Er}$ and $7.54 \mu_B/\text{Er}$, respectively in the ab -plane and along the c -axis, respectively. These values are lower than the saturation moment of Er^{3+} which is given by $g_J J(\frac{6}{5} \times \frac{15}{2} =) 9 \mu_B/\text{Er}$. Apparently higher fields are necessary to attain the full moment of Er^{3+} .

3.3.3. Crystal electric field analysis. We have applied the point charge model of crystalline electric field to the magnetic susceptibility data to get a semi-quantitative estimate of the CEF level splitting. The Er-atom in ErAl_2Ge_2 unit cell, occupies the $1a$ Wyckoff’s position with point symmetry $\bar{3}m$ (Schönflies symbol: D_{3d}) which possesses trigonal site symmetry. The crystal field Hamiltonian for rare-earth atom occupying trigonal site symmetry is given by:

$$\mathcal{H}_{\text{CEF}} = B_2^0 \mathbf{O}_2^0 + B_4^0 \mathbf{O}_4^0 + B_4^3 \mathbf{O}_4^3 + B_6^0 \mathbf{O}_6^0 + B_6^3 \mathbf{O}_6^3 + B_6^6 \mathbf{O}_6^6, \quad (1)$$

where B_n^m are the crystal field parameters and \mathbf{O}_n^m are the Stevens operators [20, 21]. In order to reduce the number of fitting parameters and for the sake of convenience, we have used the CEF Hamiltonian for the hexagonal site symmetry which is given by,

$$\mathcal{H}_{\text{CEF}} = B_2^0 \mathbf{O}_2^0 + B_4^0 \mathbf{O}_4^0 + B_6^0 \mathbf{O}_6^0 + B_6^6 \mathbf{O}_6^6. \quad (2)$$

Previously, we used the same approximation for analysing the anisotropic magnetic properties of isostructural HoAl_2Ge_2 [11]. The 16-fold ($2J + 1$; $J = 15/2$) degenerate level of free Er^{3+} ion splits into 8 doublets in the CEF of hexagonal symmetry. The magnetic susceptibility including the molecular field contribution λ is given by

$$\chi^{-1} = \chi_{\text{CEF}}^{-1} - \lambda_i, \quad (3)$$

where χ_{CEF} is CEF susceptibility. The expression for the magnetic susceptibility and magnetization based on the CEF model is given in [22, 23]. In order to analyse the inverse susceptibility in the above CEF model, we first fitted the paramagnetic inverse susceptibility to modified Curie–Weiss expression by fixing the μ_{eff} value to $9.59 \mu_B/\text{Er}$ and subtracted the resulting χ_0 value from the raw susceptibility data. Finally we plotted the inverse $(\chi - \chi_0)$ versus temperature and fitted the CEF Hamiltonian of equation (3) to the renormalized data, following the procedure applied earlier on some rare-earth

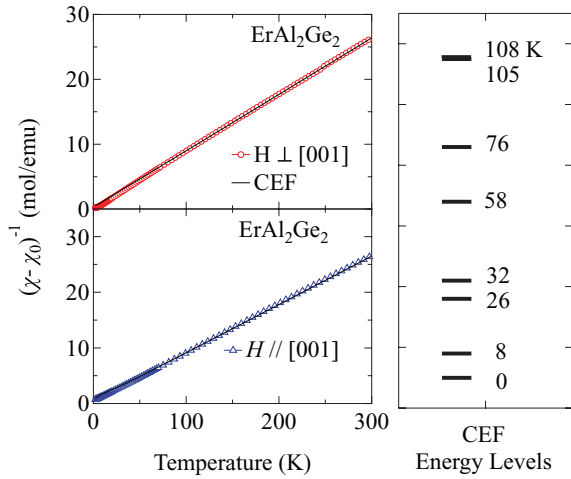


Figure 5. The crystal electric field analysis on the inverse susceptibility data. The solid lines are fit to the CEF analysis (refer to text). The estimated energy levels are also shown.

intermetallic compounds [24, 25]. The solid lines in figure 5 show the fitted inverse magnetic susceptibility based on the CEF model, with the crystal field parameters as $B_2^0 = -0.062$ K, $B_4^0 = 0.001$ K, $B_6^0 = -3.9 \times 10^{-5}$ K, $B_6^6 = 2.0 \times 10^{-5}$ K. The molecular field coefficients are $\lambda_x = -0.1$ mol emu $^{-1}$ and $\lambda_z = -0.62$ mol emu $^{-1}$. The negative sign of the molecular field constants, albeit small, supports the antiferromagnetic nature of the magnetic ordering. The corresponding energy eigenvalues of the crystal field levels are also shown in figure 5. In practice various combinations of CEF parameters B_n^m 's which furnish widely different CEF energy eigenvalues provide a good fit to the susceptibility data. However, the listed CEF parameters also qualitatively explain the magnetization data as shown in figure 4(b). The energy eigenvalues depicted in figure 5 provide the closest fit to the Schottky heat capacity (to be discussed later) and can be taken as the first order estimates. From the mean field theory, one can obtain a rough estimate of the B_2^0 parameter which is related to the paramagnetic Weiss temperature and the exchange constant by the following relation [26]

$$k_B \theta_a = \frac{1}{3} J(J+1) \mathcal{J}_{\text{ex}}^a + \frac{2}{5} \left(J - \frac{1}{2} \right) \left(J + \frac{3}{2} \right) B_2^0, \quad (4)$$

and

$$k_B \theta_c = \frac{1}{3} J(J+1) \mathcal{J}_{\text{ex}}^c - \frac{4}{5} \left(J - \frac{1}{2} \right) \left(J + \frac{3}{2} \right) B_2^0. \quad (5)$$

Assuming, an isotropic two-ion interaction $\mathcal{J}_{\text{ex}}^a = \mathcal{J}_{\text{ex}}^c = \mathcal{J}_{\text{ex}}$ and using $J = 15/2$ and the paramagnetic Curie–Weiss temperature θ_p values, obtained in section 3.3, the value of B_2^0 was estimated to be -0.092 K. Given the assumptions involved in the point charge model and the limitations of the mean field theory, this value may be considered to be in fairly good agreement with the B_2^0 value obtained from the CEF analysis. It thus provides some additional support to our final choice of crystal field parameters and the resulting crystal field levels.

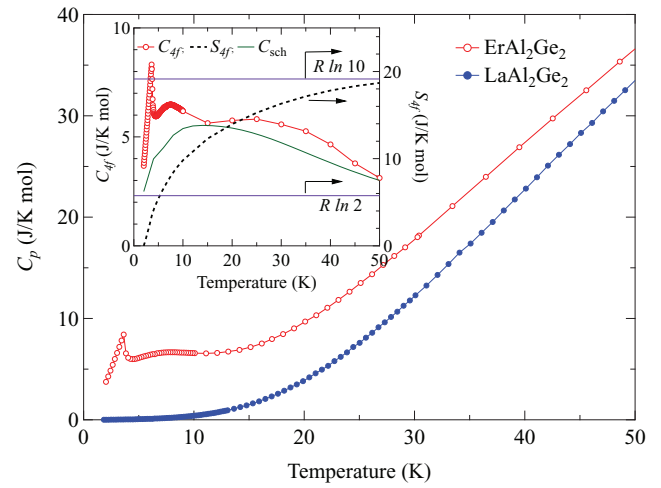


Figure 6. Temperature variation of heat capacity of ErAl $_2$ Ge $_2$ and LaAl $_2$ Ge $_2$. Inset shows the temperature variation of the 4f-derived heat capacity and the corresponding entropy of ErAl $_2$ Ge $_2$ and the solid line is the calculated Schottky heat capacity based on CEF calculations.

3.4. Heat capacity studies

The temperature dependence of the specific heat capacity of a single crystalline ErAl $_2$ Ge $_2$ and its non-magnetic reference polycrystalline LaAl $_2$ Ge $_2$ in the temperature range 2 – 50 K is shown in the main panel of figure 6. The heat capacity of the magnetic compound ErAl $_2$ Ge $_2$ is greater than the non-magnetic compound in the entire temperature range, due to the additional 4f-derived contribution to the heat capacity C_{4f} . A very sharp λ -like transition is observed at $T_N = 4$ K suggesting the bulk nature of the magnetic ordering in ErAl $_2$ Ge $_2$. We have estimated the 4f-derived contribution to the heat capacity C_{4f} , by subtracting the phononic contribution (taken to be identical to that of LaAl $_2$ Ge $_2$) from the heat capacity of ErAl $_2$ Ge $_2$ and plotted it in the inset of figure 6. Above the magnetic transition, a broad peak is observed in the magnetic part of the heat capacity, which is mainly attributed to the Schottky heat capacity arising due to the thermal population of the several low lying crystalline electric field states as the temperature is increased. Theoretically, the Schottky heat capacity can be calculated using the energy levels obtained from the CEF fitting of the magnetic susceptibility data. The expression for the Schottky heat capacity is given by the following relation:

$$C_{\text{Sch}}(T) = R \left[\frac{\sum_i g_i e^{-\frac{E_i}{T}} \sum_i g_i E_i^2 e^{-\frac{E_i}{T}} - \left(\sum_i g_i E_i e^{-\frac{E_i}{T}} \right)^2}{T^2 \left(\sum_i g_i e^{-\frac{E_i}{T}} \right)^2} \right], \quad (6)$$

where R is the gas constant, E_i is the energy in units of temperature and g_i is the degeneracy of the energy level, the summation index i runs from zero to $(n - 1)$ number of energy levels. The solid curve in the inset of figure 6, representing the CEF derived Schottky heat capacity is in a semi-quantitative agreement with the experimentally observed

values. An estimate of the entropy change with temperature has also been carried out and it is shown in the inset of figure 6. The entropy increases very rapidly and attains a value of nearly 20 J/(K mol), thus suggesting several low lying CEF states.

4. Summary

In summary, we have successfully grown the single crystals of ErAl_2Ge_2 and studied its anisotropic physical properties. From the susceptibility and magnetization data, we infer that the easy axis of magnetization is inclined more towards the ab -plane. In the simple two sub-lattice collinear antiferromagnet, the magnetic susceptibility along the easy axis should go down to zero as the temperature is decreased below T_N . However, in the present case the susceptibility along the ab -plane is larger and does not go down to zero. This suggests a possible canting of the magnetic moments and the moments are inclined more closer towards the ab -plane. A microscopic tool like neutron diffraction experiment is necessary to determine the exact orientation of the magnetic moment. The anisotropy in the magnetic susceptibility can be qualitatively explained by our CEF analysis. It has been shown that the 16 fold ($2J + 1$) degenerate level of the free Er^{3+} ion splits into eight doublets with an overall separation of just 108 K with several levels lying at low energies. The estimated crystal field energy levels account semi-quantitatively for the experimentally observed Schottky heat capacity. The electrical resistivity revealed that a superzone gap forms in ErAl_2Ge_2 below the antiferromagnetic transition. The exchange interaction, as reflected by the magnetic transition temperature in Ho and Er analogs decreases as one moves towards the higher rare-earth side, which is in accordance with the deGennes scaling. It would be interesting to study the next compound in the series TmAl_2Ge_2 where, based on the CEF theory, one can expect to see the change of the easy axis compared to ErAl_2Ge_2 and that work is planned as a future study.

ORCID iDs

Moumita Nandi  <https://orcid.org/0000-0003-4078-7875>

A Thamizhavel  <https://orcid.org/0000-0003-1679-4370>

S K Dhar  <https://orcid.org/0000-0003-3074-9058>

References

- [1] Steglich F, Aarts J, Bredl C, Lieke W, Meschede D, Franz W and Schäfer H 1979 *Phys. Rev. Lett.* **43** 1892
- [2] Dung N D, Ota Y, Sugiyama K, Matsuda T D, Haga Y, Kindo K, Hagiwara M, Takeuchi T, Settai R and Onuki Y 2009 *J. Phys. Soc. Japan* **78** 024712
- [3] Thamizhavel A, Kulkarni R and Dhar S 2007 *Phys. Rev. B* **75** 144426
- [4] Joshi D A, Nigam A, Dhar S and Thamizhavel A 2010 *J. Magn. Magn. Mater.* **322** 3363–71
- [5] Drachuck G, Böhmer A E, Bud'ko S L and Canfield P C 2016 *J. Magn. Magn. Mater.* **417** 420–33
- [6] Klüfers P and Mewis A 1984 *Z. Kristallogr.-Cryst. Mater.* **169** 135–48
- [7] Kranenberg C, Johrendt D, Mewis A, Pöttgen R, Kotzyba G, Rosenhahn C and Mosel B D 2000 *Solid State Sci.* **2** 215–22
- [8] Kranenberg C, Johrendt D and Mewis A 1999 *Z. Anorg. Allg. Chem.* **625** 1787–93
- [9] Schobinger-Papamantellos P and Hulliger F 1989 *J. Less Common Met.* **146** 327–35
- [10] Maurya A, Kulkarni R, Thamizhavel A, Bonville P and Dhar S 2015 *J. Phys. Conf. Ser.* **592** 012045
- [11] Matin M, Mondal R, Thamizhavel A, Provino A, Manfrinetti P and Dhar S 2018 *AIP Adv.* **8** 055709
- [12] Okamoto H 1993 *J. Phase Equilib.* **14** 118–9
- [13] Qin P, Chen Y, He J, He W, Nong L and Zeng L 2008 *Mater. Chem. Phys.* **109** 515–8
- [14] Elliott R and Wedgwood F 1963 *Proc. Phys. Soc.* **81** 846
- [15] Das P K, Kumar N, Kulkarni R, Dhar S and Thamizhavel A 2012 *J. Phys.: Condens. Matter* **24** 146003
- [16] Onimaru T et al 2008 *J. Phys. Soc. Japan* **77** 074708
- [17] Takabatake T, Shirase M, Katoh K, Echizen Y, Sugiyama K and Osakabe T 1998 *J. Magn. Magn. Mater.* **177** 53–4
- [18] Aoki Y, Kobayashi Y, Sato H, Sugawara H, Sechovsky V, Havela L, Prokes K, Mihalik M and Menovsky A 1996 *J. Phys. Soc. Japan* **65** 3312–6
- [19] Joshi D A, Nagalakshmi R, Dhar S and Thamizhavel A 2008 *Phys. Rev. B* **77** 174420
- [20] Stevens K 1952 *Proc. Phys. Soc. A* **65** 209
- [21] Hutchings M, Seitz F and Turnbull B 1965 *Solid State Physics: Advances in Research and Applications* ed F Seitz and B Turnbull (New York: Academic) p 227
- [22] Das P K, Kumar N, Kulkarni R and Thamizhavel A 2011 *Phys. Rev. B* **83** 134416
- [23] Das P K, Bhattacharyya A, Kulkarni R, Dhar S and Thamizhavel A 2014 *Phys. Rev. B* **89** 134418
- [24] Takeuchi T et al 2004 *J. Phys.: Condens. Matter* **16** L333
- [25] Mondal R, Bapat R, Dhar S and Thamizhavel A 2018 *Phys. Rev. B* **98** 115160
- [26] Jensen J and Mackintosh A R 1991 *Rare Earth Magnetism* (Oxford: Clarendon) p 73